



**AUTHOR(S):**

**TITLE:**

**YEAR:**

**Publisher citation:**

**OpenAIR citation:**

**Publisher copyright statement:**

This is the \_\_\_\_\_ version of proceedings originally published by \_\_\_\_\_  
and presented at \_\_\_\_\_  
(ISBN \_\_\_\_\_; eISBN \_\_\_\_\_; ISSN \_\_\_\_\_).

**OpenAIR takedown statement:**

Section 6 of the “Repository policy for OpenAIR @ RGU” (available from <http://www.rgu.ac.uk/staff-and-current-students/library/library-policies/repository-policies>) provides guidance on the criteria under which RGU will consider withdrawing material from OpenAIR. If you believe that this item is subject to any of these criteria, or for any other reason should not be held on OpenAIR, then please contact [openair-help@rgu.ac.uk](mailto:openair-help@rgu.ac.uk) with the details of the item and the nature of your complaint.

This publication is distributed under a CC \_\_\_\_\_ license.

\_\_\_\_\_

# CFD Modelling Of Pipe Erosion Due To Sand Transport

Oluwademilade Adekunle Ogunesan<sup>1\*</sup>, Hossain Mamdud<sup>1</sup>, Iyi Draco<sup>1</sup>, Mohamed Ghazi Dhroubi<sup>1</sup>

<sup>1</sup> School of Engineering, Robert Gordon University, AB10 7GJ, Aberdeen, UK

\*o.a.ogunesan@rgu.ac.uk; m.hossain@rgu.ac.uk; d.iyi@rgu.ac.uk;  
m.g.dhroubi@rgu.ac.uk

**Abstract.** Erosion caused by sand particles is a serious problem facing the oil and gas industry. Predicting pipe erosion due to sand transport is a complex process in multiphase flows due to the complex nature of the flow. Existing erosion studies are however focused on single phase flow conditions which are conservative and could lead to under- / over-engineering because actual fluid flow in pipelines is multiphase. There is therefore a need for in-depth analysis of the complex interaction between the multiphase fluid and transported sand particles.

This study employs CFD modelling techniques to investigate the complex interactions between the multiphase fluid and transported sand particles in pipes, and the subsequent effect on pipe erosion rate and location under varying operating conditions. In view of this, the Eulerian Multifluid-VOF Model coupled with Interfacial Area Transport Equations have been employed to simulate air-water two phase flow and the result shows good agreement with experimental data.

This fluid flow results have been employed in investigating sand erosion in multiphase flow through pipes. The Eulerian Multifluid-VOF model has been coupled with the Lagrangian framework for particle tracking and an appropriate erosion correlation has been employed to predict the pipe erosion rate. The pipe was observed to erode more 45 degrees into the elbow and maximum erosion rate is  $4.028 \times 10^{-6}$  kg/m<sup>2</sup>s. These results are in acceptable range when compared to available data. Erosion rate was also observed to be transient.

**Keywords:** Erosion, Erosion rate, Multiphase Flow, CFD.

## 1 Introduction

The ever growing demand for oil and gas due to the increasing world population pushes the oil and gas industry to increase production and supply of hydrocarbon. Hence the need to explore extreme environment where access to crude is very challenging. One of these challenges is sand production. Though technology advancement has led to the design of various sand control mechanism, sand particles are still being produced and transported alongside the fossil fuel, leading to problems of blockage, pressure drop and pipe erosion.

The most important infrastructure that links the production field to the processing field is the pipelines. Most prolific hydrocarbon reservoirs are prone to produce sand, therefore oil and gas pipelines will contain streams of liquid, gas and solid particles. Understanding the complex interaction between the sand particles, fluid and pipe wall is important in order to get to know the effects of the sand particles impinging on the pipe wall (erosion).

Multiphase gas-liquid flow occurs in many industries such as chemical, petroleum, process and manufacturing amongst others. This necessitates the need for predicting tools to aid the design of facilities [1]. Various physical scenarios can be observed in gas-liquid multiphase flows, and this behaviour can vary as the multiphase pattern changes. As the flow behaviour changes, so does the erosion rate and pattern. Many different methods have been employed to investigate erosion in multiphase flow from experimental to analytical to CFD, but CFD as a comprehensive tool gives room for obtaining more information about these scenarios and the physical parameters influencing them as well as the complex interactions between the phases (gas-solid-liquid) [2]. Erosion prediction in multiphase flow is very difficult due to the complexity of the flow and it solely depends on the flow patterns in question. It also becomes more complicated tracking particles entrained in multiphase flows [3].

Many researchers such as [3-12] have investigated erosion in pipelines and multiphase flow, many models have been proposed, developed and are currently in use. While most of these are based on empirical data, some were developed mathematically. These models do not give room to obtain all parameters of interest but in recent years CFD has become a more prominent tool in predicting pipe erosion.

Chen et al. [13] employed CFD technique to calculate erosion in elbows for different multiphase flow patterns by introducing an effective sand mass ratio and a single phase flow. Results showed good agreement with available data, however, effects of particle interaction was assumed negligible. Parsi et al. [14] presented results from CFD simulation of gas dominant multiphase flow in elbows from their study of churn flow. They employed three different superficial gas velocities of 10.1, 18.3 and 27.1 m/s while that of the liquid remained constant at 0.3 m/s. Sand particle sizes 150 and 300 $\mu$ m were used. Erosion model developed by Mansouri et al. [15] showed very good agreement with experimental data. The authors concluded that CFD cannot only predict erosion pattern but also the maximum rate in acceptable range. However, particle loading was assumed to be sufficiently low. Dense flow is frequently encountered in practice, hence the particle-particle interaction cannot be ignored anymore. A CFD-DEM-based liquid-particle two-phase flow simulation to predict erosion rate and location in 90, 60 and 45 degree pipe elbows was conducted by Chen J et al. [16], the 90 degree elbow was observed to be the most erosive and results agreed well with experimental data.

Literature review has shown that there is still limited understanding available in the study of erosion in complex multiphase flows as well as the transition between them, from very low gas velocities to high gas velocities, this has informed the objectives of this study. This study is focused on the investigation of sand particle erosion in pipes where varying flow patterns are expected in vertical –horizontal pipe with a standard 90 degree elbow. The flow modelling results generated from the numerical simulation and preliminary results of the pipe erosion analysis are presented in this paper.

## 2 Numerical Modelling

### 2.1 Governing Equations

The Multifluid-VOF model of ANSYS Fluent 18.0 was employed for the transient simulation of air-water multiphase flow, with the effects of gravity incorporated, while the solid phase was modeled with the Discrete Phase Model (DPM), the final erosion rate at the pipe bend has been accounted for by employing the erosion model developed by Oka et al. [17].

The hybrid Multifluid-VOF model is a combination of the Eulerian-Eulerian model which solves separate mass and momentum equations for the individual phases, and VOF to capture the evolution of the interfaces between them. A single pressure field is shared between the two phases. To account for the momentum and energy transfers through the interface between the liquid and gas phases, the Interfacial Area Concentration (IAC) correlation was incorporated in this hybrid model. The IAC captures the bubble breakage and coalescence within the flow. Assuming no mass transfer between the two phases, the governing equations are written as shown in equations 1 to 3.

- The continuity equation for the gas phase is;

$$\frac{\partial \rho_i \alpha_i}{\partial t} + \nabla \cdot (\alpha_i \rho_i \vec{v}_i) = 0 \quad (1)$$

$$\sum_q^n \alpha_i = 1 \quad (2)$$

Where  $\alpha_i$ ,  $\rho_i$  and  $\vec{v}_i$  are the volume fraction, density and velocity of the individual phases.

- The momentum equation for the gas phase is;

$$\frac{\partial(\alpha_i \rho_i \vec{V}_g)}{\partial t} + \nabla \cdot (\alpha_i \rho_i \vec{V}_g \vec{V}_g) = -\alpha_i \nabla p + \nabla \cdot \tau_i + \alpha_i \rho_i \vec{g} + \vec{F}_{ij} \quad (3)$$

Where  $P$  and  $\tau_i$  are the pressure and stress-strain tensor of the individual phases,  $g$  is acceleration due to gravity and  $\vec{F}_{ij}$  is the interfacial force between the phases.

One advantage of using this hybrid model is that individual velocity information of the phases can be extracted and employed for erosion analysis. The right hand side of equation 3 accounts for forces such as pressure gradient, interfacial forces, virtual mass force, drag force, lift force, turbulent dispersion and wall lubrication force. Closure of the momentum equations was accounted for using the RNG k- $\epsilon$  model.

- The transport equation for interfacial area concentration, IAC, is given as;

$$\frac{\partial(\rho_g X_p)}{\partial t} + \nabla \cdot (\rho_g \vec{u}_g X_p) = \frac{1}{3} \frac{D\rho_g}{Dt} X_p + \frac{2}{3} \frac{m_g}{\alpha_g} X_p + \rho_g (S_{RC} + S_{WE} + S_{TI}) \quad (4)$$

Where  $X_p$  is the interfacial area concentration and  $\alpha_g$  is the gas volume fraction. The first two terms on the right hand are the gas bubble expansion due to compressibility

and mass transfer,  $m_g$  is the mass transfer rate into the gas phase per unit mixture volume.  $S_{RC}$  and  $S_{WE}$  are coalescence sink terms due to random collision and wake entrainment respectively.  $S_{TI}$  is the breakage source term due to turbulent impact. The source and sink terms are accounted for with the Hibiki-ishii model which is based on the works of Ishii et al. (2000).

- The DPM model to track the sand /solid phase is;

$$m \frac{dV}{dt} = F_D + F_P + F_V + F_G + F_{Other} \quad (5)$$

Where  $F_D$  is the drag force,  $F_P$  is the force due to pressure gradient,  $F_V$  is the virtual mass (this is the force required to accelerate the fluid surrounding the particles and  $F_G$  is the force due to gravity.  $F_{Other}$  accounts for other forces acting on the particles.

- Erosion model developed by Oka et al. (1995) is;

$$ER = \rho_w k_0 f(\alpha) (Hv)^{k_1} \left( \frac{|u_p|}{V'} \right)^{k_2} \left( \frac{d_p}{d'} \right)^{k_3} \quad (6)$$

$$f(\alpha) = (\sin \alpha)^{n_1} [1 + Hv(1 - \sin \alpha)]^{n_2} \quad (7)$$

Where  $\rho_w$  is the density of the pipe wall,  $Hv$  is the Vickers hardness of the pipe wall (GPa),  $d' = 326 \mu m$  (particle reference diameter),  $V' = 104 m/s$  (reference velocity),  $k_0 = 65 \times 10^{-9}$  and  $k_1 = -0.12$ , are model constants while  $k_3 = 0.19$  the diameter exponent.  $k_2$ ,  $n_1$  and  $n_2$  can be determined by Equations (8), (9) and (10) respectively.

$$k_2 = 2.3(Hv)^{0.038} \quad (8)$$

$$n_1 = 0.71(Hv)^{0.14} \quad (9)$$

$$n_2 = 2.4(Hv)^{-0.94} \quad (10)$$

## 2.2 Flow Domain

The computational geometry (Fig. 1) consists of consists of 3m vertical and 1.9m horizontal pipes, upstream and downstream a standard 90 degree elbow respectively. Flow of fluid is from upward vertical to horizontal. Pipe diameter and elbow radius of curvature are 76.2mm and 1.5 respectively. A monitoring surface was created 1m before the elbow from where Void Fraction data was extracted and compared with experimental data.

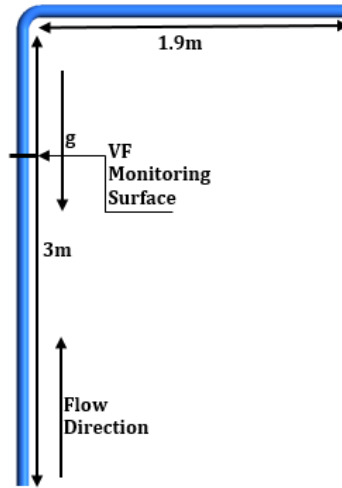


**Fig. 1.** Computational vertical - horizontal geometry with a standard 90 degree elbow

### 2.3 Mesh/Grid Generation

A structured grid was generated across the flow domain as shown in Fig. 2a. Three different grids were considered in conducting a mesh sensitivity analysis in this study. The details of the grids employed are shown in Table 1. The inlet surface was split into two (Fig. 2b), the gas phase was introduced via the middle of the pipe inlet (red) while the liquid phase was introduced circumferentially (blue).

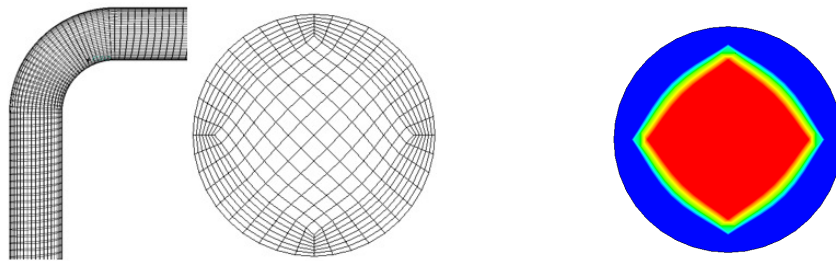


**Fig. 2.** a) Cross-sectional slice of the grid(s) employed, b) Injection of the phases via the inlet – red and blue indicates air and water respectively.

**Table 1.** Number of Cells Used In Different Grids

Grid Name	Total Number of Cells
Mesh 1	117882
Mesh 2	200640
Mesh 3	312192

## 2.4 Flow Conditions

Six air-water flow conditions were considered for this study as shown in Fig. 3. These conditions were observed on the flow regime map employed in Parsi et al. [14], the test cases cut across 6 different flow patterns that can be observed in vertical pipes. The superficial liquid velocity ( $V_{sl}$ ) was kept constant at 0.3m/s while the superficial gas velocity ( $V_{sg}$ ) was varied. Table 2 shows the air conditions employed in this study while water velocity is 0.3m/s.

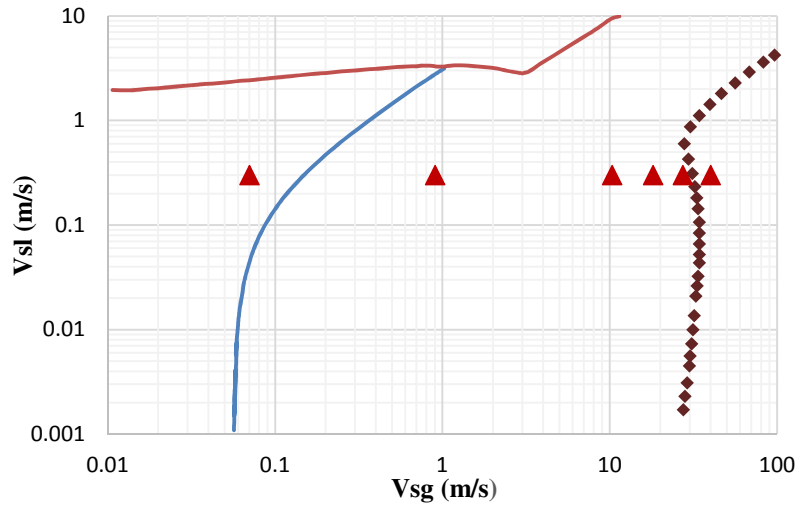


Fig. 3. Flow conditions on flow pattern map

Table 2. Air-Water Simulation Conditions

Case No.	1	2	3	4	5	6
$V_{sg}(m/s)$	0.07	0.9	10.3	18.1	27.3	40
$V_{sl}(m/s)$	0.3	0.3	0.3	0.3	0.3	0.3

## 3 Results and Discussion

Six different gas velocities were studied at a constant water velocity, this is to vary between the features of different flow patterns. The contour plots, time series and probability distribution function (PDF) of the measure void fractions are presented. 3-D transient simulations were conducted at an appropriate time step size of 0.0001s, the simulations were performed long enough for the cases to achieve steady state conditions.

### 3.1 Mesh Sensitivity Study

The effect of change in grid size on the mean and standard deviation of the time series of void fraction of case 3 ( $V_{sg} = 10.3\text{m/s}$  and  $V_{sl} = 0.3\text{m/s}$ ) is shown on Table 3. This case is the validation case for this study. Based on these results, Mesh 2 was employed for the purpose of this study. Results from test case 3 which is the validation case were employed for this analyses.

**Table 3.** Mesh Independence Study

	<b>Experiment</b>	<b>Mesh 1</b>	<b>Mesh 2</b>	<b>Mesh 3</b>
<b>Mean</b>	0.75	0.65	0.72	0.71
<b>SD</b>	0.10	0.14	0.12	0.14

### 3.2 Time Series of Average Void Fraction and Contour Plots

Time series of void fraction have a distinct nature of occurrence in different flow patterns, although it has the following main features irrespective of the flow pattern; time series of void fraction exhibit cyclic fluctuations that shows the sudden increase or drop in cross-sectional average void fraction across a monitoring surface, and an increase in superficial gas velocity ( $V_{sg}$ ) leads to a drop in the amplitude of the fluctuations. In this section the time series of void fraction and void fraction contour plot in the 6 test cases are presented.

On the contour plot of case 1 (Fig. 4a), small and less uniformly distributed gas bubbles with no coalescence are observed in a continuous liquid flow stream. This type of condition is expected at relatively low gas and high liquid flow rates and it is representative of the bubbly flow pattern which occurs at conditions with the gas phase moving at a relatively low speed and the liquid phase moving at a high velocity. The cyclic fluctuations of the time series of VF is also shown in Fig. 4b. These fluctuation shows a representative trend of bubbly flow as observed in previous studies by Taitel et al. [18], Costigan and Whalley [19] & Lowe and Rezkallah [20].

Contour plot from case 2 (Fig. 5a) shows an alternating gas pockets of varying lengths separating a liquid flow stream. The alternating gas pockets are referred to as Taylor Bubbles while the discontinuous liquid streams are referred to as liquid slugs [2] [19] [20]. This pattern is referred to as slug flow and occurs over a wide range of gas and liquid velocities. These characteristics is also observed on how the fluctuations are represented on the time series of VF (Fig. 5b). The high void fraction values indicates the passage of Taylor bubbles across the monitoring plane while the low void fractions are indicative of the liquid slugs.

Fig. 6a, 7a and 8a are contour plots from cases 3, 4 and 5. Here the boundaries between the liquid and gas phases cannot be ascertained as there is the presence of waves and discontinuous gas cores. The features of slug and annular low can be observed here because it occurs in-between the two flows, the huge waves being the liquid slug in slug flow and the developing gas core as seen in annular flows. This type of flow is

referred to as intermittent flow or churn flow as its natural occurrence is between slug and annular flow, and due to its undefined boundaries. To the best of the author's knowledge, there is limited published material on churn flow due to its complex nature of occurrence. Some researchers also consider it to be fundamentally annular in nature with large disturbance waves carried by the gas flow [19]. The time series of VF for cases 3, 4 and 5 are shown in Fig. 6b, 7b and 8b, the unstable nature of the cyclic fluctuations observed here can be attributed to the complex and undefined nature of the liquid and gas phases. Case 3 is the validation case for this study and results generated have shown good agreement with the experimental data from Parsi et al. [14]. The huge wave observed by Parsi et al. [14] can also be seen in Fig. 6a.

The contour plot of case 6 (Fig. 9a) shows a dominant and continuous gas core (red), this is a feature observed in annular flow. The high gas velocity forms a uniform gas core at the middle of the flow domain and pushes the liquid phase moving at a lower speed towards the pipe wall to form a thin liquid film. According to [19] and [20], the average void fraction in annular flow is between 0.8 and 0.9, this is observed in case 6 as shown in Fig. 9b.

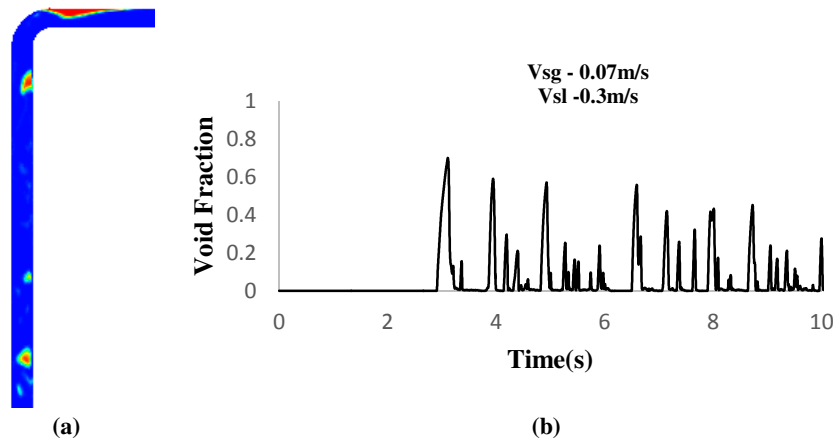
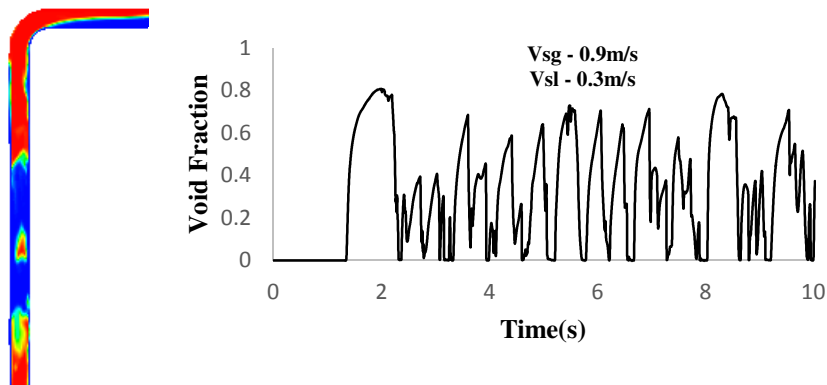
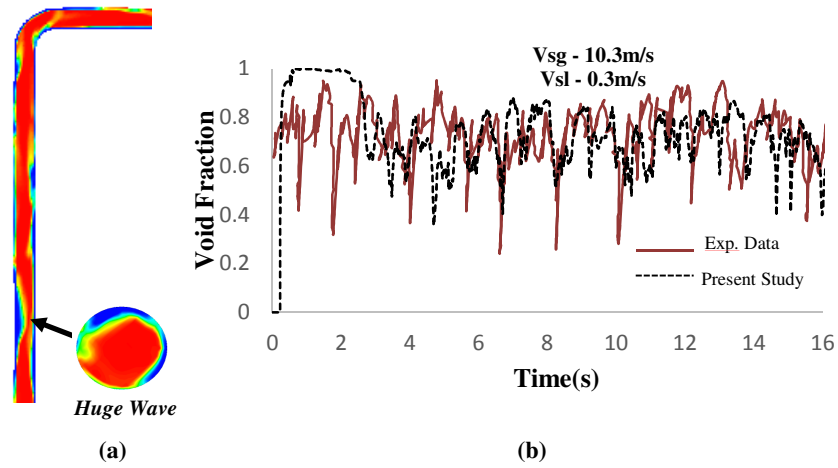


Fig. 4. Case 1 - a) Contour plot, b) Time series of void fraction.



(a) (b)

**Fig. 5.** Case 2 - a) Contour plot, b) Time series of void fraction.



**Fig. 6.** Case 3 - a) Contour plot, b) Time series of void fraction.

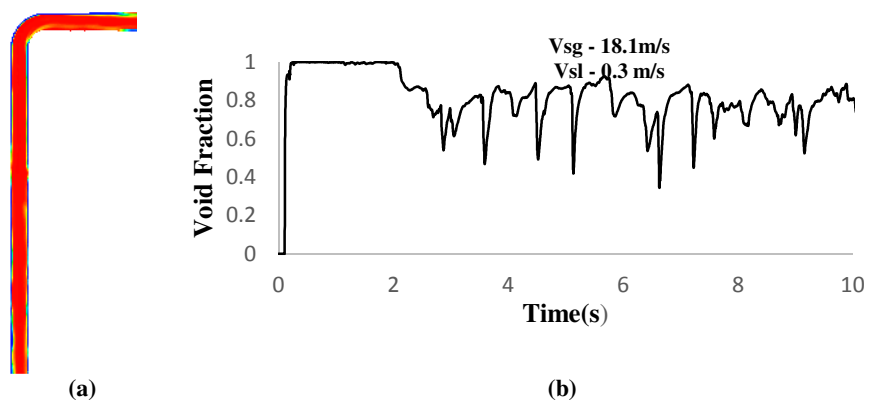


**Fig. 7.** Case 4 - a) Contour plot, b) Time series of void fraction.

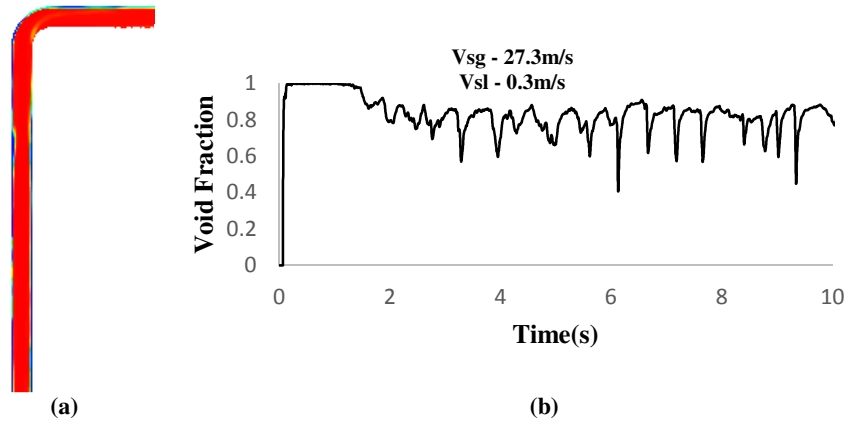


**Fig. 8.** Case 5 - a) Contour plot, b) Time series of void fraction.

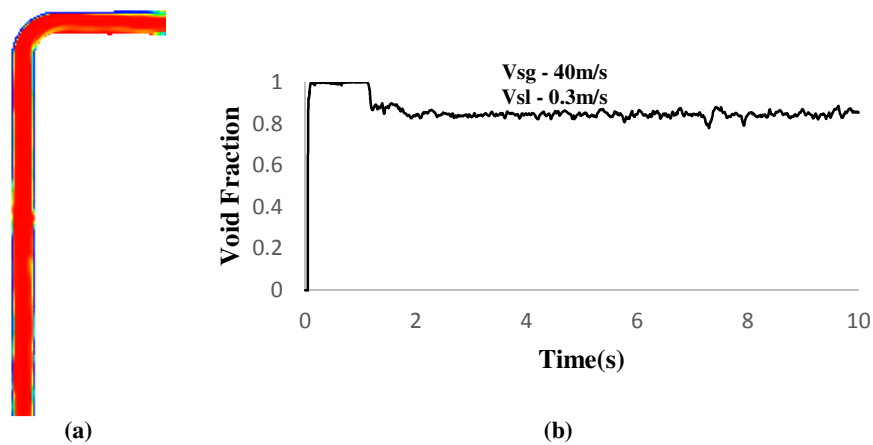


**Fig. 9.** Case 6 - a) Contour plot, b) Time series of void fraction.

It is further inferred from Fig. 4 - 9 that with a constant  $V_{sl}$  of  $0.3\text{m/s}$ , as the  $V_{sg}$  increases, the cyclic pattern of time series shrinks i.e a reduction in the alternating passage of the phases. Hence the gas phase becomes more dominant and its average volume fraction increases and becomes more stable. This is indicative of a transition between the flow patterns. A change in the presence of the gas phase between cases across the monitoring surface is shown in Fig. 10.

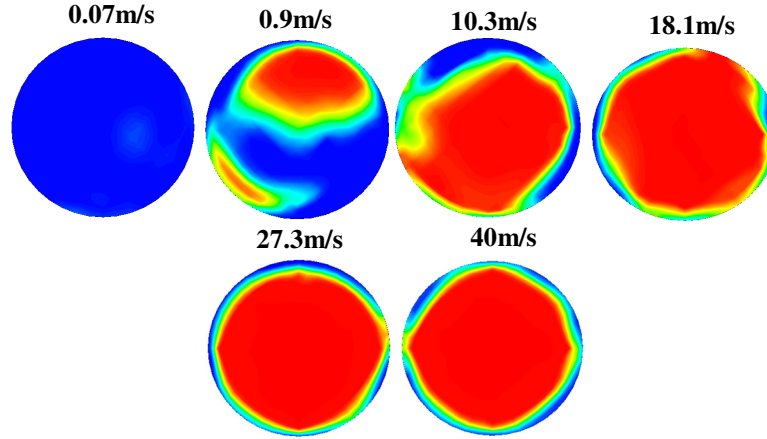


**Fig. 10.** Contour of changes in void fraction across the cases (Vsl remained constant at 0.3m/s).

### 3.3 Mean Void Fraction

This is computed from the time averaging of the time series of cross sectional average void fraction over the simulation run time for the six cases. Table 4 shows the mean void fractions of cases 1 to 6. The mean void fraction of the validation case (Case 3) is scarcely distinguishable from the experimental data presented by Parsi et al. [21].

The ranges of mean void fraction observed from all cases are similar to those observed by Costigan and Whalley [19] and Lowe and Rezkallah [20].

**Table 4.** Mean void fraction

Case No.	Vsg(m/s)	Vsl(m/s)	Mean VF	Exp
1	0.07	0.3	0.08	
2	0.9	0.3	0.36	
<b>3</b>	<b>10.3</b>	<b>0.3</b>	<b>0.72</b>	<b>0.75</b>
4	18.1	0.3	0.79	
5	27.3	0.3	0.81	
6	40.0	0.3	0.85	

### 3.4 Probability Density Function

The probability Density Function (PDF) shows the probability that a continuous random variable acquires a specific value [21]. Statistical analysis of the behaviour of void fraction is one method that can also be used to further ascertain flow patterns under normal gravity conditions. It reveals the probability of each void occurring in the fluid. According to [19-20] every flow pattern exhibit a specific PDF signature based on the

fluctuation of its fluid phases. In this study, the *ksdensity* function of MATLAB was used to generate the PDF curves of average void fraction.

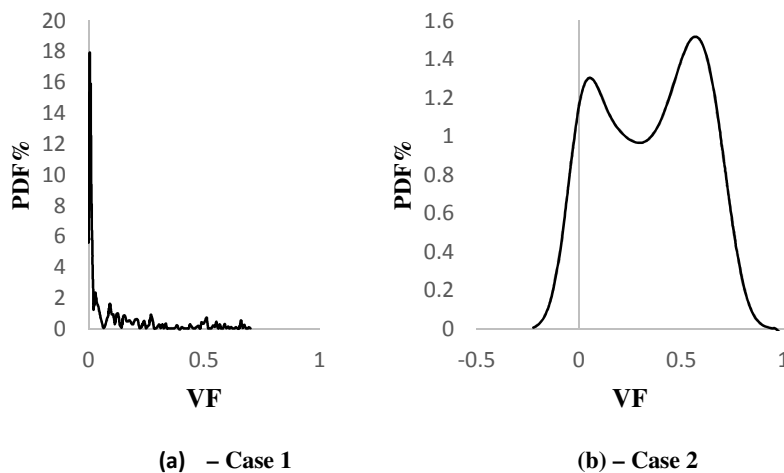
The bubbly flow is characterised by a PDF curve with a single narrow peak at the low void fractions. This shows the small or minor fluctuations which corresponds to the passage of bubbles about the monitoring surface. According to Lowe and Rezkallah [20], a PDF with a single peak less than 0.2 is indicative of bubbly flow. This condition is observed from the PDF curve of case 1 as shown in Fig. 11a.

In slug flow, the PDF of time series average void fraction has two peaks, one at the low void fractions and another at higher ones. These peaks represents the periodic passage of the two specific features of slug flows; the Taylor bubble at high void fractions and liquid slug at low void fractions. This is observed in case 2 as shown in Fig. 11b.

Churn flow is characterised by high void fraction with random dips and lows with no clear boundaries between the phases. The low dips are very short lived, hence the unstable nature of the slug. Churn flow is characterised by a PDF curve with a single peak at high void fractions and a broad tail at the low void fractions, the single peak at high void fraction is indicative of the flow's proximity to annular flow and the broad tail represents the passage of unstable slugs. According to Lowe and Rezkallah [20], a typical PDF curve of churn flow is between an average VF of 0.6 and 0.9, this can be observed in cases 3, 4 and 5 (Fig. 11**Error! Reference source not found.**c, d and e). Although results generated conform to standard features of the different flow patterns in literature, case 3 was also compared with experimental data for validation purpose and a good agreement was observed.

In annular flow conditions, the PDF shows a single peak at a very high void fraction with a narrow tail. The PDF curve is typically between 0.8 and 0.9 [20], these features are clearly observed in the PDF curve of case 6 (Fig. 11**Error! Reference source not found.**f).

As the superficial gas velocity,  $V_{sg}$ , increases, significant changes in the PDF curve is observed, the effect of this change in gas velocity, PDF and flow pattern on the pipe erosion at the elbow due to sand transport will also be analyzed in the next phase of this study.



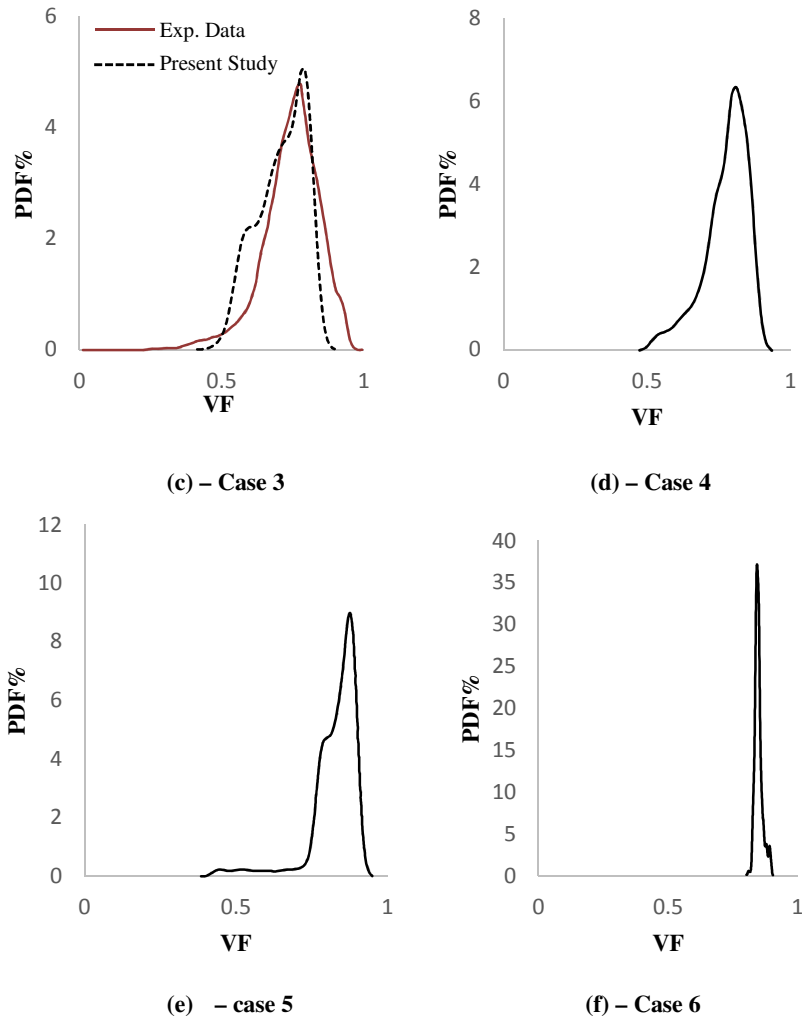


**Fig. 11.** Probability Density Function (PDF) Curves

### 3.5 Preliminary Erosion Analysis in Multiphase Flow

The Lagrangian framework is coupled with the Eulerian-Multifluid VOF frame to account for the behaviour of sand particles in the multiphase flow patterns. The Discrete Phase Model (DPM) was employed for the particle tracking and erosion model developed by Oka et al. [17] was used to calculate the erosion rate at the pipe bend. The drag force which determines the particle behaviour / motion depends on the properties of the continuous flow field.

The framework described above has been applied to test case 3 ( $V_{sg} = 10.3\text{m/s}$  and  $V_{sl} = 0.3\text{m/s}$ ) to extract the maximum erosion rate and location at the pipe bend. The sand particle diameter was  $300\mu\text{m}$ . A two-way transient particle tracking simulation

was carried out for multiphase flow. The erosion contour, maximum erosion location and particle tracks are shown in Fig. 12.

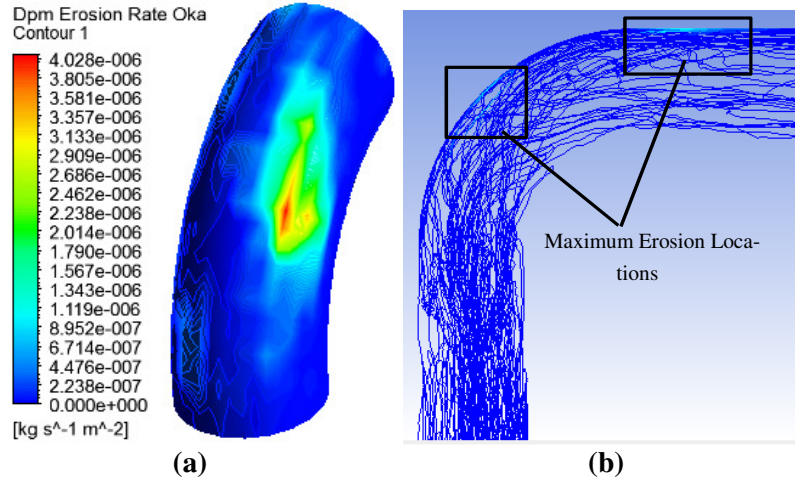


**Fig. 12.** a) - Erosion Contour; b) - Particle Tracks with erosion locations

The pipe was observed to erode more at 45 degrees into the elbow, this spreads towards the right side of the elbow and extrados (Fig. 12). Fig. 12b shows the particle tracks and the erosion location at the pipe bend and elbow extrados are highlighted, these are locations where the sand particles impinge most on the internal pipe wall. The maximum erosion rate at the elbow is  $4.028 \times 10^{-6}$  kg/m<sup>2</sup>s. These initial results show appropriate agreement with experimental data, erosion contour and erosion rate from the works of Parsi et al. [14] and [22]. However, it was observed that the maximum erosion rate is transient while the location remained relatively consistent (Fig. 13), hence, the next phase of this study will investigate how the particle tracks and erosion rate changes with time and volume fraction.

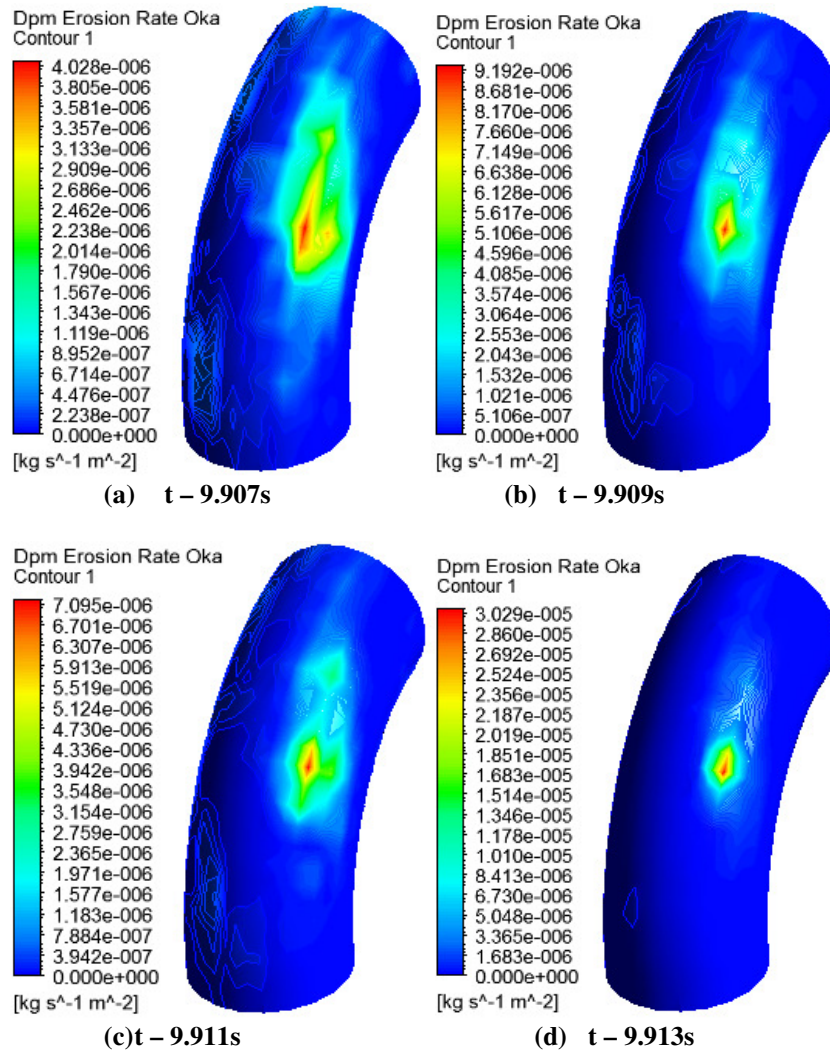


Fig. 13. Changes in Erosion Rate and Location with Time (Time Interval - 0.002s)

#### 4 Conclusions

CFD was used to simulate air-water multiphase flow with the use of the Eulerian-Multifluid VOF framework in a 76.2mm diameter pipe. Sand particles were injected into the flow domain and the particles were tracked within Discrete Phase Model (DPM) frame, end erosion rate and location at the bend were accounted for.

The numerical multiphase flow physics set up has been appropriately validated with experimental data, and employed to simulate different air-water two-phase flow patterns. The instantaneous void fraction time series and PDF of void fraction has shown qualitative and quantitative agreement with available experimental data and literature.

Preliminary erosion results also show good prospects when compared to the available experimental data, however it was observed that the erosion rate at the pipe bend is transient. Further erosion analyses will focus on establishing the transient nature of the erosion rate in pipe elbows. The effects of change in flow pattern (volume fraction) on pipe erosion rate, location and particle tracks would also be investigated. This procedure would be extended to the other flow patterns under study and a correlation between the erosion rates in different flow patterns would be established.

## References

1. O. Shoham, Mechanistic Modelling of Gas-Liquid Two-phase Flow in Pipes, 2006.
2. M. Parsi, K. Najmi, F. Najafifard, S. Hassani, B. S. McLaury and S. A. Shirazi, "A comprehensive review of solid particle erosion modeling for oil and gas wells and pipelines applications," *Journal of Natural Gas Science and Engineering*, vol. 21, pp. 850 - 873, 2014.
3. B. S. McLaury, S. A. Shirazi, V. Viswanathan, Q. H. Mazumder and G. Santos, "Distribution of Sand Particles in Horizontal and Vertical Annular Multiphase Flow in Pipes and the Effects on Sand Erosion," *Journal of Energy Resources Technology*, vol. 133, no. 2, p. 023001, 2011.
4. B. S. McLaury, S. Shirazi, J. R. Shadley and E. Rybicki, "How operating and environmental conditions affect erosion," 1999.
5. B. S. McLaury and S. A. Shirazi, "An alternate method to API RP 14E for predicting solids erosion in multiphase flow," *Journal of energy resources technology*, vol. 122, no. 3, pp. 155 - 122, 2000.
6. Q. H. Mazumder, S. A. Shirazi and B. S. McLaury, "A mechanistic model to predict erosion in multiphase flow in elbows downstream of vertical pipes," in *NACE International - CORROSION*, 2004.
7. Q. H. Mazumder, S. A. Shirazi and B. McLaury, "Experimental investigation of the location of maximum erosive wear damage in elbows," *Journal of Pressure Vessel Technology*, vol. 130, no. 1, p. 011303, 2008.
8. Q. H. Mazumder, S. A. Shirazi and B. S. McLaury, "Prediction of solid particle erosive wear of elbows in multiphase annular flow-model development and experimental validations," *Journal of Energy Resources Technology*, vol. 130, no. 2, p. 023001, 2008.
9. Y. Zhang, B. S. McLaury, S. A. Shirazi, E. F. Rybicki and S. Nesic, "Predicting sand erosion in slug flows using a two-dimensional mechanistic model," in *CORROSION 2011*, 2011.
10. N. Kesana, J. Throneberry, B. McLaury, S. Shirazi and E. Rybicki, "Effect of Particle Size and Viscosity on Erosion in Annular and Slug Flow," in *ASME 2012 International Mechanical Engineering Congress and Exposition*, 2012.

11. R. E. Vieira, N. R. Kesana, S. A. Shirazi and B. S. McLaury, "Experiments for Sand Erosion Model Improvement for Elbow in Gas Production, Low-Liquid Loading and Annular Flow Conditions," in *NACE International*, Houston, Texas, 2014.
12. R. E. Vieira, M. Parsi, N. R. Kesana, S. A. Shirazi and B. S. McLaury, "Effects of Flow Pattern and Flow Orientation on Sand Erosion in Elbows for Multiphase Flow Conditions," in *NACE International - CORROSION 2015*, 2015.
13. X. Chen, B. S. McLaury and S. A. Shirazi, "A comprehensive procedure to estimate erosion in elbows for gas/liquid/sand multiphase flow," *Journal of Energy Resources Technology*, vol. 128, no. 1, pp. 70 - 78, 2006.
14. M. Parsi, M. Agrawal, V. Srinivasan, R. E. Vieira, C. F. Torres, B. S. McLaury and S. A. Shirazi, "CFD simulation of sand particle erosion in gas-dominant multiphase flow," *Journal of Natural Gas Science and Engineering*, pp. 1-13, 2015.
15. A. Mansouri, H. Arabnejad, S. Karimi, S. A. Shirazi and B. S. McLaury, "Improved CFD modeling and validation of erosion damage due to fine sand particles," *Wear*, vol. 338, pp. 339-350, 2015.
16. J. Chen, Y. Wang, X. Li, R. He, S. Han and Y. Chen, "Erosion Prediction Of Liquid-Particle Two-Phase Flow In Pipeline Elbows Via CFD-DEM Coupling Method," *Powder Technology*, vol. 275, pp. 182-187, 2015.
17. Y. Oka, K. Okamura and T. Yoshida, "Practical estimation of erosion damage caused by solid particle impact Part 1: Effects of impact parameters on a predictive equation," *Wear*, vol. 259, pp. 95-101, 1995.
18. Y. Taitel, D. Bornea and A. Dukler, "Modelling Flow Pattern Transitions For Steady Upward Gas-Liquid Flow In Vertical Tubes," *AIChE Journal*, vol. 26, pp. 345-354, 1980.
19. G. Costigan and P. Whalley, "Slug Flow Regime Identification From Dynamic Void Fraction Measurements In Vertical Air-Water Flows," *International Journal Of Multiphase Flow*, vol. 23, no. 2, pp. 263-282, 1997.
20. D. Lowe and K. Rezkallah, "Flow Regime Identification In Microgravity Two-Phase Flows Using Void Fraction Signals," *International Journal Of Multiphase Flow*, vol. 25, pp. 433-457, 1999.
21. M. Parsi, M. Agrawal, V. Srinivasan, R. Vieira, C. Torres, B. McLaury, S. Shirazi, E. Schleicher and U. Hampel, "Assessment of a hybrid CFD model for simulation of complex vertical upward gas-liquid churn flow," *Chemical Engineering Research and Design*, vol. 105, pp. 71-84, 2016.
22. M. Parsi, R. Vieira, N. Kesana and B. McLaury, "Ultrasonic measurements of sand particle erosion in gas dominant multiphase churn flow in vertical pipes," *Wear*, Vols. 328-329, pp. 401-413, 2015.
23. B. S. McLaury, S. A. Shirazi, V. Viswanathan, Q. H. Mazumder and G. Santos, "Distribution of Sand Particles in Horizontal and Vertical Annular Multiphase Flow in Pipes and the Effects on Sand Erosion," *Journal of Energy Resources Technology*, vol. 133, no. 2, p. 023001, 2011.